Applied Acoustics **27** (1989) 163–201

Ocean Propagation Models

C. H. Harrison

YARD, Scientific House, 40–44 Coombe Road, New Malden, Surrey KT3 4QF, UK

ABSTRACT

Four approaches to underwater sound propagation modelling are reviewed including rays, normal modes, Green's function integral, and parabolic equation. Specific programs are discussed. Particular reference is made to the problems in running models and the applicability in various regimes, especially deep-water environments.

1 INTRODUCTION

The wave equation and the Helmholtz equation occur in many branches of physics, and the basic types of solution are always the same. However, the problems in different fields vary tremendously because of emphasis on different types of source, receiver, environment, geometry and so on. Whereas propagation of light and radar in air is relatively straightforward, underwater sound propagation can be extremely complex and calculations may require several hours of computation on a CRAY-size computer. In the underwater environment there are many different types of problem, some far simpler than others. These include detecting distant ships or submarines, echo sounding, short baseline location, seismic surveying and acoustic tomography.

A typical problem of interest in this paper is to calculate intensity (and phase) from a receiver somewhere in the water column separated by distances of 1–100 km in water of depth 100–5000 m. The water is usually assumed to be stratified (i.e. depth-dependent sound speed with constant

Applied Acoustics 0003-682X/89/$03·50

density), the sea surface is treated as a perfect pressure-release reflector, and the sea bed may be treated as a reflector or multiple-layered refracting medium with arbitrary density, sometimes demanding inclusion of shear wave effects and surface scattering. A number of models are capable of tackling range-dependent environments in which the bathymetry and sound speed structure are allowed to vary relatively slowly in range. A few can handle three-dimensional effects to a limited extent.

The aim of this paper is to provide a review of some of these programs for the non-specialist in underwater acoustics. The examples are taken from various underwater environments, and are woven into the discussion which emphasises some of the practical problems in running the models. Some rules-of-thumb are suggested for deciding which model is appropriate.

The review also refers to some comparisons, tests and a few unusual applications. The models considered are some of the well known ones developed with physical understanding in mind and minimal approximation or empiricism. These are: GRASS (ray); SNAP and SUPERSNAP (normal mode); SAFARI and FFP (Green's function); and PAREQ and IFD (parabolic equation).

2 REGIMES AND ENVIRONMENTS

It is difficult to appreciate the complexity of propagation modelling without understanding the many environments and propagation regimes. These are distinguished partly according to the various mathematical approaches and partly according to oceanography and geophysics; many references discuss the subject.[1-5] On top of this there are variants of these environments and other applications of the usual models such as propagation from air to water,[6-8] propagation in air,[9] seismic modelling,[10] ultrasound,[10] and radio propagation over undulating terrain (the multiple-knife-edge diffraction problem which is often tackled fairly crudely[11]). Despite the complications of diffraction and wave treatment the phenomena that need to be modelled can be understood very simply by considering the corresponding ray paths.

2.1 Shallow water

The term 'shallow water' is often taken as synonymous with the Continental Shelf where it has special strategic significance. For shipping-line frequencies of less than a few hundred hertz, where the wavelength is a significant proportion of the water depth, shallow water behaves like a waveguide in which propagation is dominated by bottom reflection. Ray paths may be relatively steep, and consequently relatively straight, in the water column so that the influence of the water column velocity profile is minimal. On the other hand, the propagation may be strongly influenced by the structure of the sediment and the underlying rock since sudden changes in velocity and density and the inevitable gradual increase in velocity with depth provide strong reflections, particularly if there is a critical angle, and upward refracted paths with potentially low losses.

Absorption in the sediment increases with frequency and typical values[12] are between 0·05 and 0·5 dB/m/kHz, i.e. at 100 Hz the loss might reach 10 dB after a 1 km path length. By contrast, the losses in water are extremely low, although they still rise with frequency. At 100 Hz a 10 dB loss is reached after 10 000 km. The corresponding ranges for 10 kHz, though, are 10 m for sediment and 10 km for water.

An additional factor in shallow water is the possibility of a solid rock sea bed which supports shear waves. Under certain conditions the boundary between the solid and fluid layer (whether water or sediment) may exhibit interface waves, the effects of which are significant for sources and receivers near the bottom.[13] A common phenomenon is the result of the fact that the shear critical (grazing) angle, if it exists, is always smaller than the compression wave critical angle, so that there is a tendency for energy to leak into the bottom by generation of downward-propagating shear waves. This effect can be screened out or toned down by an intermediate layer of fluid sediment between the rock and water.

2.2 Deep water

In deep water propagation can be very complex because there are so many different types of path. The sound speed increases roughly linearly with depth, temperature and salinity. The salinity in the oceans usually plays a minor role, although in the polar regions, in landlocked seas such as the Baltic, and in the vicinity of some ocean fronts and eddies, there are significant effects. In the North Atlantic in winter there is typically a well mixed warm surface layer, several hundreds of metres thick which, when superimposed on the depth effect, causes a minimum in sound speed at about 1000 m with a maximum at several hundred metres. Above this maximum there is a surface duct where rays from a shallow source can be trapped by upward refraction and surface reflection.

Below the maximum is a deep sound channel centred on 1000 m, bounded entirely by refraction. However, to make use of this regime both source and receiver need to be at depths below the maximum. Steeper rays from a near-surface source travel more deeply, and the roughly linear increase of velocity with depth causes upward refraction. There is often a slight focusing effect so that the rays that nearly hit the bottom bunch up near the surface at around

60 km. This region of sudden high intensity is known as a 'convergence zone' and it repeats at multiples of about 60 km.

Two extremely important phenomena resulting from refraction are caustics, where initially adjacent rays converge, and shadow zones, where adjacent rays diverge. In the velocity profile just described a shallow source might form a wedge-shaped shadow extending from the velocity maximum, which defines the bottom of the surface duct, to the downward-refracted ray below. Conversely, a shallow receiver would not be able to see a source in this shadow zone via the direct refracted path. However, a downward-looking or omnidirectional beam receiver would also be sensitive to bottom reflections (bottom bounce) or bottom refracted paths which would fill the shadow in. Consequently, the nature of the sea bed can be extremely important for near-surface sources and receivers.

The Atlantic in summer has a more gradual change in temperature with depth, so that the profile is closer to a parabola. In all seasons very shallow surface ducts (30 m or so) may form by mixing during the day, and these may have significant effects above a few kHz where the duct thickness is greater than a few wavelengths. From the modelling point of view it should be remembered that the surface mixing that gives rise to the isothermal layer constituting the duct is caused by wind and wave action, which necessarily makes the surface rough. At frequencies of several kHz (wavelength less than 1 m), scattering effects are certainly significant and difficult to model from first principles since the mechanisms are a complicated mix of surface shape effects and surface-modulated volume scattering by entrained bubbles.[1,14]

A topic of increasing interest is Arctic and under-ice propagation.[15,16] Here the profile is virtually linear, giving rise to an upward-refracting deep surface duct. Two of the complications added by ice cover are the roughness of the lower surface and the effects of shear waves propagating in the ice.

2.3 Range dependence

An improvement over the assumption of a stratified medium is made by including changes of velocity profile and water depth (bathymetry) with range. Slow changes in bathymetry may deflect bottom-reflected paths into the sound channel and vice versa. Relatively abrupt changes are encountered with ocean fronts where there may be significant changes over a horizontal distance of 100 m. As will be seen, there are a number of models that can handle range dependence, but not many that can cope with abrupt changes. In any case, it is extremely hard to validate range-dependent models against real data, and it is also difficult to devise analytical benchmarks.

2.4 Three-dimensional effects

Clearly, refraction effects are also possible in the horizontal plane, especially in the vicinity of ocean fronts. Increasing computer power has made it possible, for instance, to investigate the horizontal effects of an eddy passing across a fixed source[17] (made tangible by cine film of a very large number of runs showing intensity at a fixed depth in the horizontal plane). A less obvious horizontal bending, shadowing and focusing effect is caused by propagation across a slope, each bottom reflection causing a slight horizontal deflection.[18-20] In fact, the horizontal curvature can be viewed as stemming from the differing phase velocities of the vertical normal modes in the varying-depth waveguide.[21]

Although there are clearly three-dimensional effects which are important for some of the time, propagation modelling in this domain is still in its infancy. A lot of recent effort has gone into deriving exact solutions for the wedge,[22] and a conical seamount,[23] and confirming these experimentally.[24] There is no truly general three-dimensional propagation model although there are some close approaches.[25]

3 MODELLING TREATMENTS

The two most widely used concepts in understanding propagation problems are rays and normal modes. Naturally, the approaches to modelling have followed these concepts, but emphasis in the past 20 years has been on computer-intensive wave treatments which are broader in scope than the normal mode approach. Nevertheless, in reconciling results from different types of model one still has to resort to simple ideas and calculations using rays, modes, images, flux and so on.

It is natural to use whichever approach is computationally most efficient for the circumstances, and so in shallow water or in a duct where there are vast numbers of reflected rays it is most useful to think in terms of modes.[26] Conversely, at short range or in deep water there may be only a few 'eigenrays' connecting the source and receiver but a very large number of modes, so it is advantageous to think in terms of rays.

One can group propagation models into seven types as follows, although the first four are in more common usage than the subsequent two, and the last is much more special-purpose.

(1) ray tracing;
(2) normal mode;
(3) Green's function types;

(4) parabolic equation types;
(5) coupled-mode types;
(6) finite element types;
(7) empirical.

The first six types have been reviewed by De Santo[27] and the first four by Jensen.[28] This review will restrict itself to the first four types although some references are given for coupled mode,[29-33] finite element[27,34,35] and empirical[1,36-38] models.

Examples of computer codes are given below: a more complete list is given in references[39-42]:

ray,	GRASS,[43,44] PLRAY[45];
mode,	SNAP,[46] SUPERSNAP[47];
Green's function,	SAFARI,[48-50] FFP[51,52];
PE,	PAREQ,[53,54] IFD.[55,56]

There are other models such as FACT[57] and RAYMODE[58] that do use ray concepts, although transmission loss is calculated without going through the motion of tracing the rays. These models are designed to be used 'hands-off' and so mode calculations are inserted automatically as appropriate, source and receiver may be swapped, etc. Therefore for the research user it is often difficult to control what calculations are executed.

A brief description of the four approaches is given below, but more detail can be found in Refs 2–4, 27–28 and 59–61. All four can be derived from the inhomogeneous Helmholtz equation, i.e. the wave equation with a point harmonic source,

$$\nabla^2\phi + k^2(\mathbf{r})\phi = -\delta(\mathbf{r}) \tag{1}$$

where $k = \omega/c$ is the local wavenumber.

3.1 Ray tracing

In the limit of high frequencies the Helmholtz equation can be reduced to an Eikonal equation which describes the path swept out by rays in three dimensions.[60] In an inhomogeneous medium the changes in direction cosine (α, β, γ) for an incremental step, $\mathrm{d}s$, in the ray are given by[39]:

$$\begin{aligned}
\mathrm{d}\alpha &= -\frac{\mathrm{d}s}{c}\left[(1-\alpha^2)\frac{\partial c}{\partial x} - \beta\alpha\frac{\partial c}{\partial y} - \gamma\alpha\frac{\partial c}{\partial z}\right] \\
\mathrm{d}\beta &= -\frac{\mathrm{d}s}{c}\left[(1-\beta^2)\frac{\partial c}{\partial y} - \gamma\beta\frac{\partial c}{\partial z} - \alpha\beta\frac{\partial c}{\partial x}\right] \\
\mathrm{d}\gamma &= -\frac{\mathrm{d}s}{c}\left[(1-\gamma^2)\frac{\partial c}{\partial z} - \alpha\gamma\frac{\partial c}{\partial x} - \beta\gamma\frac{\partial c}{\partial y}\right]
\end{aligned} \tag{2}$$

A convenient assumption in a marine environment (and several others, such as air) is that the medium is horizontally stratified, and then one can directly calculate range, r, and delay time, t, from

$$r = \int \cot\theta \, dz \qquad t = \int (c \sin\theta)^{-1} \, dz \tag{3,4}$$

using Snell's law, that $c \sec\theta$ is constant for each ray. Also, the radius of curvature of the ray, R, can be written in terms of velocity, its gradient and the grazing angle at one depth as

$$R = c \sec\theta / (dc/dz) \tag{5}$$

The intensity, I, relative to the intensity at unit distance I_0 is usually calculated from the horizontal spread of the rays. With an initial ray elevation angle and sound speed θ_0, c_0 and a local angle and sound speed θ, c, the formula is

$$I = I_0 c_0 / (cr \sin\theta \, |\partial r / \partial \theta_0|) \tag{6}$$

With the exception of the vicinity of focuses and caustics this gives adequate representation of the loss. In these regions corrections can be applied.[43]

There are a number of other useful ray or hybrid concepts such as ray invariants,[18-21] and flux.[26,62,63] These are related to the WKB formula for mode number[64] and the adiabatic approximation,[21,32] and are useful when the medium is range-dependent. Although these approaches have not formed the basis of computer codes they can provide insight through analytical or numerical calculations. Simple calculations may also be based on the method of images[65] in some circumstances. The concept of 'fuzzy' rays has also been developed recently.[66]

Frequency-dependent effects are sometimes included in ray-tracing models, but without detailed corrections to the phase of bottom reflections, ray tracing cannot compete with normal-mode models in shallow water. A rule of thumb is that ray tracing can be used when the water depth or the thickness of a refracting duct is many wavelengths. One disadvantage of ray tracing is that many rays need to be computed to provide a reasonable spread at the receiver end. Another is that ray computations need to be made at all ranges out to the specified receiver. This is not so with normal mode models. An advantage is that rays can easily be traced through varying velocity profiles and over undulating sea bed. Directionality of the source can be inserted, in principle, by selecting particular initial ray angles and weighting accordingly.

3.2 Normal mode

The Helmholtz equation can be separated in range and depth assuming cylindrical symmetry and vertical stratification. The solution of the resulting one-dimensional equation in depth can be expressed as the sum of the discrete normal modes (i.e. the solution of a homogeneous Helmholtz equation) and one or more branch cut integrals.[27] The acoustic pressure is given by

$$p = \frac{i}{4} \sum_n \phi_n(z_s)\phi_n(z_r)\mathrm{H}_0^{(1)}(K_n r) \tag{7}$$

where ϕ_n are the normal modes evaluated at the source and receiver depths z_s and z_r, and K_n are the eigenvalues. The discrete sum represents loss free modes equivalent to up- and down-going rays travelling at a well defined angle given by the horizontal wavenumber $K_n = k(z)\cos\theta(z)$. The branch cut integrals represent lossy modes travelling at lower wavenumbers (steeper angles), and the contributions that are only effective at short range where the up- and down-going waves do not balance properly yet.

The normal modes are calculated by choosing trial values of K_n and using numerical techniques such as Runge–Kutta iteratively, until the boundary conditions are matched at depths zero and infinity with the correct number of zero crossings.[67] These methods are adequate for shallow water in which there are a small number of modes, and they are the basis of the model SNAP. In deep water the far larger number of modes is a problem in itself, but the close packing in wavenumber coupled with the refracting ducts means that low-order modes are likely to contain upward- and downward-decaying portions which lead to stability problems with standard shooting methods such as Runge–Kutta. Porter and Reiss[47,68] have used a finite difference approach which is adopted in SUPERSNAP to formulate the mode calculation as an algebraic eigenvalue problem which is more stable. Ferla *et al.* report some high-frequency normal mode calculations in deep water.[69]

Strictly speaking, because the normal mode method is based on separation of range and depth variables, it cannot be used unless the medium is horizontally stratified. Nevertheless, if the range variations in velocity profile and depth are only slight, the energy in each mode remains constant as the mode propagates (the adiabatic approximation[32,33]). In fact, the rays corresponding to a particular mode become steeper when the water becomes shallower because of the reflections from the sloping bottom. These steeper rays in shallower water correspond to exactly the same mode as the original one in deep water, although the mode shape will have squashed vertically to fit into the water column. Weak variations of velocity profile and water depth are incorporated into SUPERSNAP via the adiabatic approximation.

Various other effects have been included in normal-mode models. The effect of different bottom types may be incorporated through the velocity profile, density and absorption.[67] Shear wave effects,[70] and surface or bottom roughness[71] can also be treated.

Other variants of the normal-mode programs include those which compute the complete spectrum of modes. This is necessary under certain circumstances, for instance when the last mode has passed cut-off (discrete-mode programs would give zero result) or when there are downward-propagating shear waves, weak reflections or when the receiver is close to the source. The extra computation involves evaluation of a branch cut integral.[27,72–74] It is probably more straightforward to use the Fast Field Program in this case since it routinely evaluates the whole spectrum of modes.

3.3 Green's function solutions

The complete solution of the inhomogeneous Helmholtz equation for a stratified medium can be written as the Hankel transform of the vertical Green's function

$$\phi(r, z_r) = \int_0^{\infty} \dot{G}(K, z_r, z_s)\, \mathrm{J}_0(Kr) K \, \mathrm{d}K \tag{8}$$

This is the basis of the Fast Field Program (FFP)[51,52] and SAFARI.[48–50] In both programs the bulk of the computation time is taken up with calculation of the Green's function G (as a function of horizontal wavenumber K). The Hankel transform is approximated by a Fourier transform which is implemented by FFT algorithm. The original FFP used the Thomson–Haskell method at each K to evaluate G by matching the solutions at each layer boundary and the source. SAFARI starts with the same equations but uses a global matrix scheme to solve for all K and all layers simultaneously.

The Green's function, as a function of K for fixed source and receiver depth, is an intermediate output of the programs, and it is extremely useful not only for checking performance but for providing insight into the physics. The discrete and virtual modes are shown in Fig. 1(a), and the corresponding transmission loss is shown in Fig. 1(b). The distinction between the Green's function and the normal modes can be seen by analogy with a violin string stretched across the water column. The normal modes are the shapes of the violin string at its many resonances (the violin frequency corresponds to the horizontal wavenumber). Between resonances the amplitude is zero, and so the sequence is discrete. The Green's functions are the shapes of the violin string when driven by a harmonic source at some particular position along the length (i.e. the source depth). These exist for any frequency of the harmonic source, although there will be a large amplitude at each resonance.

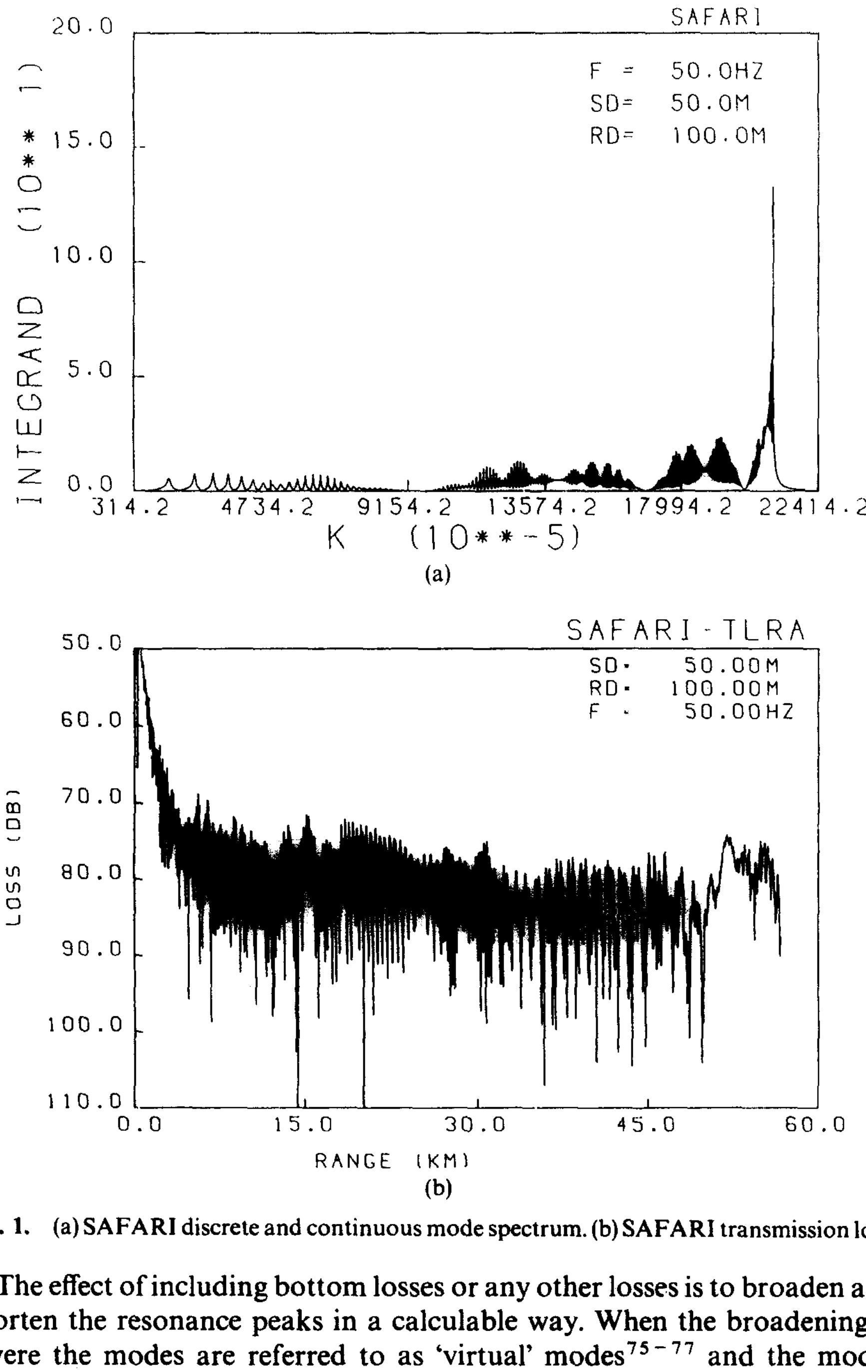

Fig. 1. (a) SAFARI discrete and continuous mode spectrum. (b) SAFARI transmission loss.

The effect of including bottom losses or any other losses is to broaden and shorten the resonance peaks in a calculable way. When the broadening is severe the modes are referred to as 'virtual' modes[75–77] and the modes decay exponentially with range (as is apparent from considering the Fourier transform of an exponential). Similarly, the method can handle mode cut-offs, shear waves in solid layers (sediment, seabed, or ice) and near field as opposed to far field. SAFARI (and FFP) is a very powerful program for research because it gives an accurate solution of the wave equation for mixed liquids and solids (including compression, shear and interface waves[13]), at any range including the near field, above, below or near mode cut-offs. SAFARI has been implemented by Schmidt on an array processor, making calculations with multiple frequencies, sources and receivers feasible. This has led to the ability to produce synthetic seismograms and contour plots of ultrasonic beams.[10] Its two shortcomings are that it can (so far) only deal with horizontally stratified media, and its computation time is rather long despite the efficiency of the code.

3.4 Parabolic equation

The parabolic equation takes a different starting point from SAFARI, FFP and the normal-mode programs. For waves travelling predominantly within a small range of angles (not necessarily horizontal) one can approximate the elliptic wave equation to a parabolic equation by taking out the main oscillating part of the solution in a function $S(r)$. Thus the velocity potential ϕ can be written in terms of a slowly varying function, ψ, of range and depth[28,54]:

$$\phi = \psi(r, z)S(r) \tag{9}$$

and the parabolic equation is

$$\frac{\partial^2 \psi}{\partial z^2} + 2ik_0 \frac{\partial \psi}{\partial r} + k_0^2(n^2 - 1)\psi = 0 \tag{10}$$

where the wavenumber $k = k_0 n$ has been written in terms of an arbitrarily chosen constant k_0 (the 'reference wavenumber', related to the 'reference sound speed' by $k_0 = \omega/c$) and the refractive index $n = c_0/c$ which is assumed to be slowly varying. It is evident from eqn (10) that if ψ is completely defined over a vertical line at some given range then ψ and $\partial^2\psi/\partial z^2$ are known, and consequently $\partial\psi/\partial r$ is known. Therefore, ψ can be calculated for all z at the next range step $r + \mathrm{d}r$, and so on. This 'marching' solution allows one to start with a known wavefront at some point and follow its horizontal progress as it diffracts through the medium and around the humps in the sea bed. Clearly, this approach can cope with horizontal variations in velocity profile and variations in depth.[78] A limitation is that it needs to be started up some way away from the source. For this purpose a normal-mode program is often used. An alternative is to assume the initial amplitude distribution to be a Gaussian function of depth, centred on the true source location.[28,55]

Equation (10) can be converted into manageable form by taking vertical

Fourier transforms to give the split-step-Fourier algorithm[54] which is used in PAREQ:

$$\psi(r+\Delta r, z) = \exp(\mathrm{i}k_0(n^2-1)\Delta r/2)\mathscr{F}^{-1}\{\exp(-\mathrm{i}\Delta r s^2/2k_0)\mathscr{F}(\psi(r,z))\} \quad (11)$$

The process of recalculating ψ at successive vertical planes is almost identical to the propagation of Huygen's wavelets, and in fact the above formula can be derived from the Kirchhoff approximation treating the plane at r as a diffraction screen. The various diffraction terms can be identified here simply by taking the Fourier transform of both sides of eqn (11) and writing the right-hand side as a convolution. Since the inverse FT of $\exp(-\mathrm{i}\Delta r s^2/2k_0)$ is $(k_0/\mathrm{i}\Delta r 2\pi)^{1/2}\exp(\mathrm{i}k_0 z^2/2\Delta r)$, the result is

$$\psi(r+\Delta r, z) = \left(\frac{k_0}{\mathrm{i}\Delta r 2\pi}\right)^{1/2}\exp(\mathrm{i}k_0(n^2-1)\Delta r/2) \times \int_{-\infty}^{\infty}\psi(r,z')\exp\{[\mathrm{i}k_0(z-z')^2]/2\Delta r\}\,\mathrm{d}z'$$

Given the field on the vertical plane at r the second term in the integral is precisely the Fresnel diffraction term in passing from an arbitrary point (r, z') on the first screen to the observation point on the second at $(r+\Delta r, z)$. The exponential term outside the integral corrects the phase already included in $S(r)$ (i.e. $k_0 r$, see eqn (9)) by adding in the phase due to the slowly varying refractive index but taking out $k_0 r$. The result, $k_0\Delta r(n-1)$ is equal to $k_0\Delta r(n^2-1)/2$ to first order since n is always very close to unity. The multiplier turns into the usual $k_0/2\pi\mathrm{i}\Delta r$ of the Kirchhoff approximation when allowance is made for the other dimension of the diffraction screen (horizontal, out of the plane of propagation) which supplies an extra $(k_0/2\pi\mathrm{i}\Delta r)^{1/2}$ term.

The method has been extended to wider angles (40–60°) and stronger bottom interaction by using finite difference methods, and one such model is Implicit Finite Difference (IFD).[79] There have been developments in which density is treated more comprehensively.[80] A number of operator techniques for manipulating the parabolic equation have been presented at Yale.[81] Recent extensions include calculating the field in a uniform[82] or sheared[83] current, and close approaches to three-dimensional modelling.[25,84–86]

3.5 Model comparisons

There seems to be a law of nature that says that modellers do not go to sea and experimentalists avoid using advanced models. Therefore, empirical propagation laws tend to be extremely simple, whereas advanced models go largely unverified against trials data. There are many good reasons for this.

One is that transmission loss is very sensitive to environmental parameters, and measuring *all* the quantities in the sea trial demanded by the model and also guaranteeing to fulfil all the conditions of validity of the model in the trial is almost always impossible exactly. Therefore honest comparisons are difficult, although by varying some of the unknown parameters one can probably obtain a reasonable fit. Nevertheless, an area that does have scope for controlled tests is the reconciliation of existing models with themselves and other analytical solutions. Indeed, it is important to reach a consensus and map out regions of validity before attempting to make comparisons with trials data.

Inter-model comparisons are occasionally made in the literature. Jensen *et al.*[28,87,88] have compared SNAP, FFP and PAREQ. Gilbert *et al.*[29] have compared a normal mode model (COMODE) with a coupled mode model (CUPYL) and IFD. Stickler[73] has made comparisons between FFP and normal-mode solutions that include various branch cut integrals. A number of parabolic equation corrections have been compared in Refs 89–93. Some comparisons have been made by Tolstoy[92] between the parabolic equation and ray tracing in a focusing environment. A methodology for comparison and choice in models is given by De Santo[27] (pp. 121–34).

There have also been a number of workshops and special conference sessions based on model comparisons. The AESD workshop[94] compared some wave treatment models, including FFP, discrete and continuous normal-mode models and the parabolic equation. Another workshop at NORDA[95] concentrated on parabolic equation methods. More recently, there have been the ASA sessions organised by Felsen at Anaheim[96] on benchmarks, and on tests against some range-dependent and three-dimensional analytical solutions.[97]

4 PRACTICAL LIMITATIONS AND TUNING

Having briefly reviewed the mode of operation of the models it is useful to look at some of the more practical limitations. These depend on validity in the given regime or environment, computation time and very often a lot of fine tuning and user experience. As well as the oceanographic and geo-acoustic inputs, which are themselves often difficult to define, most models have numerical inputs which need to be chosen by experience or trial and error. For instance, ray-tracing models require a ray density at the source; parabolic equation models require a reference sound speed and an understanding of the angle limits and constraints on medium variability; SAFARI requires various compromises to be made in numerical integration. One can usually devise simple formulae as an aid to choosing a starting point, but there is no substitute for repeating runs with altered numerical inputs until convergence is reached.

The following discussions are restricted to GRASS (ray), SNAP and SUPERSNAP (normal mode), SAFARI (Green's function) and PAREQ and IFD (parabolic equation). The comments are aimed at deep-water environments with source and receiver within a few hundred metres of the surface.

4.1 GRASS

It is obvious that the chosen ray density at the source must provide adequate ray coverage at distant points of interest. However, it is not always easy to predict what that density should be without a trial run. Ray traces with coarse and fine ray densities for an identical shallow surface duct are shown in Figs 2(a) and (b). The apparent size of the wedge-shaped shadow zone is quite different in the two cases. To a certain extent the worries are illusory because these rays (surface-reflected) do not contain much energy, but the incoherently added intensity (Fig. 2(c)) shows steps corresponding to the wide ray spacing in range, even for the high-density example. This kind of problem arises when the ray location at a distance is very sensitive to initial ray angle, i.e. $|\partial r/\partial\theta_0|$ is large, but this is exactly the condition that the intensity contribution is low. Whether or not the result is important depends on whether or not there are stronger contributions from elsewhere.

The obvious solution is to carry on increasing the ray density, but one penalty is increased numerical error, and another more practical limitation is computation time, which is roughly proportional to total range covered and number of rays.

Although GRASS is essentially a high-frequency approximation, the 'coherent' option sums rays with regard to their phase and is capable of showing some frequency dependence other than simple absorption effects. In principle, a ray treatment can handle bottom reflections and bottom-refracted paths, but GRASS cannot handle both correctly. One choice is to use a compromise reflection loss curve which attempts to cover both cases, but this cannot possibly treat the horizontal offset associated with the refracted path correctly. Another is only to use the model with the true reflection loss curve in the case where refracted paths are non-existent or extremely weak. The converse case where refracted paths dominate over reflected paths cannot be handled, despite the fact that refracted rays can be traced. This is because the sediment layer would have to be treated as part of the water column, and GRASS does not have the facility to include absorbing layers in the water.

In a duct ray treatments are valid as long as the duct supports a

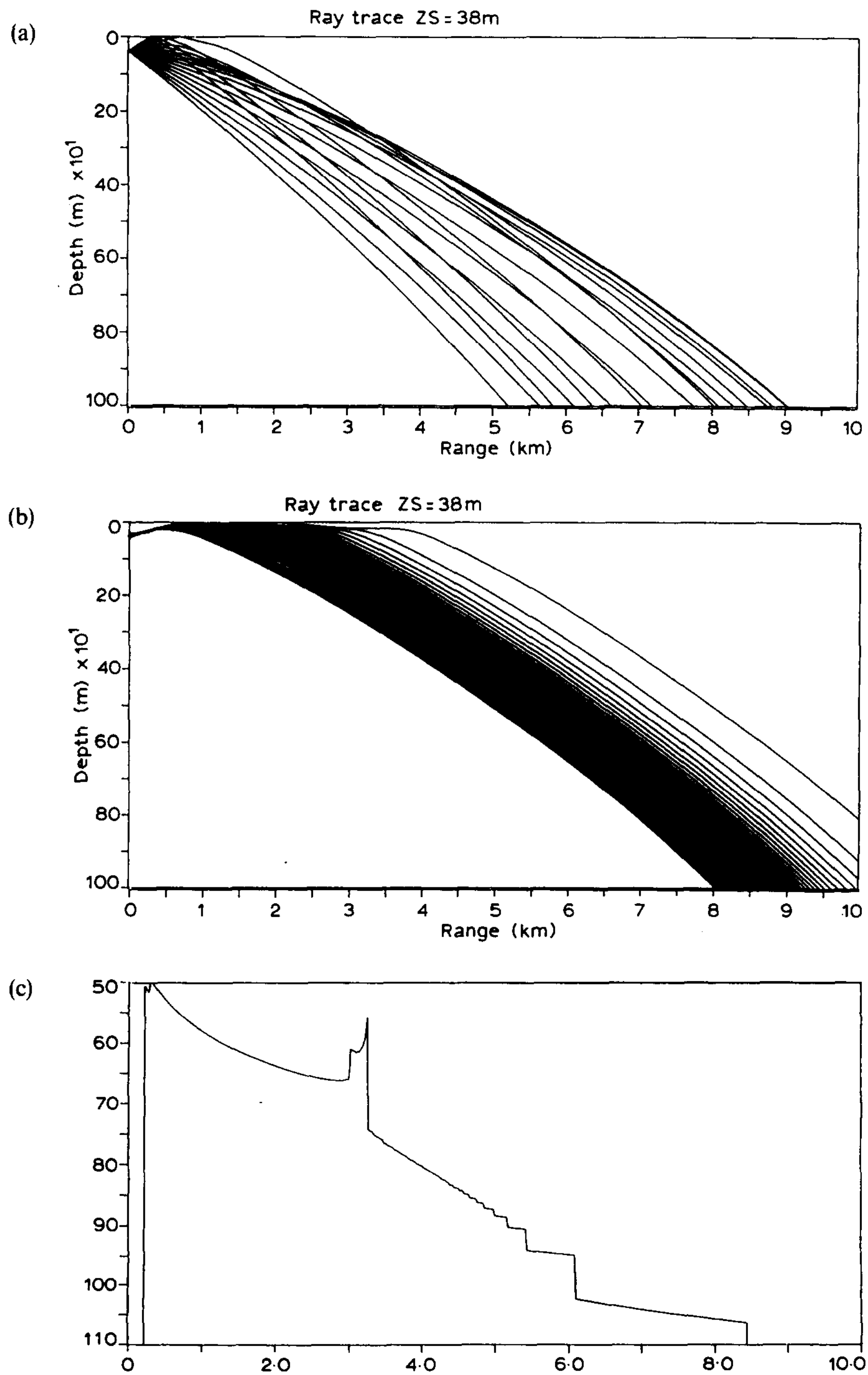

Fig. 2. (a) Coarse ray trace: 1 ray/degree; 16° spread. (b) Fine ray trace: 100 ray/degree; 1° spread. (c) Transmission loss showing steps due to finite but small ray spacing.

substantial number of modes (i.e. definitely greater than one, but not necessarily an extremely large number). Thus, treating the duct crudely as a rectangular well of height h, the mode number is related to ray angle by $2H \sin\theta = n\lambda$. For weak ducts with velocity contrast, Δc,

$$\sin\theta = (1 - c^2/(c+\Delta c)^2)^{1/2} \simeq (2\Delta c/c)^{1/2} \tag{12}$$

and a rough formula for the cut-off frequency (i.e. $n = 1$) is

$$f^2 = c^3/8h^2\Delta c \tag{13}$$

For instance, ray treatment in a surface duct with $\Delta c = 4$ m/s and $h = 500$ m requires frequencies to be well above 20 Hz. In fact, since the duct cross-section is closer to linear than rectangular, the values of h and Δc should be reduced to compensate, so that the cut-off frequency is two or three times higher. Better approximations to the formula may be made using the WKB phase integral[1] for n. The cut-off frequency for the complete water column is usually far lower, and for typical frequencies ray treatments are valid in deep water (provided that some allowance is made for Lloyd's mirror, the bottom dipole effect, etc. as appropriate). The cut-off frequency is now roughly

$$f^2 = [4H^2(c_0^{-2} - c_1^{-2})]^{-1} \tag{14}$$

where H is the total depth and the larger velocity spread is defined by the limits c_0 and c_1. For $c_0 = 1500$ m/s, $c_1 = 2000$ m/s and $H = 4000$ m the cut-off frequency is 0·3 Hz.

Above the mode cut-off the dependence of intensity on mode number is weak, because although the number of modes increases in proportion to frequency the wavenumber in the denominator of the mode sum formula (originating from the square of the Hankel function $H_0(K_n r)$ in eqn (7)) also increases in proportion to frequency. So, apart from some saw-tooth effects with very low mode number the response is flat. A more important effect for sources and receivers removed from the centre of the duct is the frequency-dependent reduction in mode amplitude near the boundaries. Crudely, the intensity for one mode is proportional to $\sin^2\gamma_n z_s \sin^2\gamma_n z_r$, and with both source and receiver near the surface this reduces to $\gamma_n^4 z_s^2 z_r^2$, where (in terms of the horizontal wavenumber, K_n, and the wavenumber in the medium, k)

$$\gamma_n = (k^2 - K_n^2)^{1/2} = (2\pi f/c)\sin\theta_n \tag{15}$$

Thus intensity will rise with the square of frequency until saturation when $\sin^2\gamma_n z$ approaches 1 for most modes. This can only be modelled with GRASS by a very large number of coherent rays.

A clear indication of the importance of modal effects at frequencies as high as 5 kHz (in typical shallow surface ducts) is shown by the comparison of Fig. 3(a) (an IFD intensity contour run on a CRAY II) with Fig. 3(b) (ray

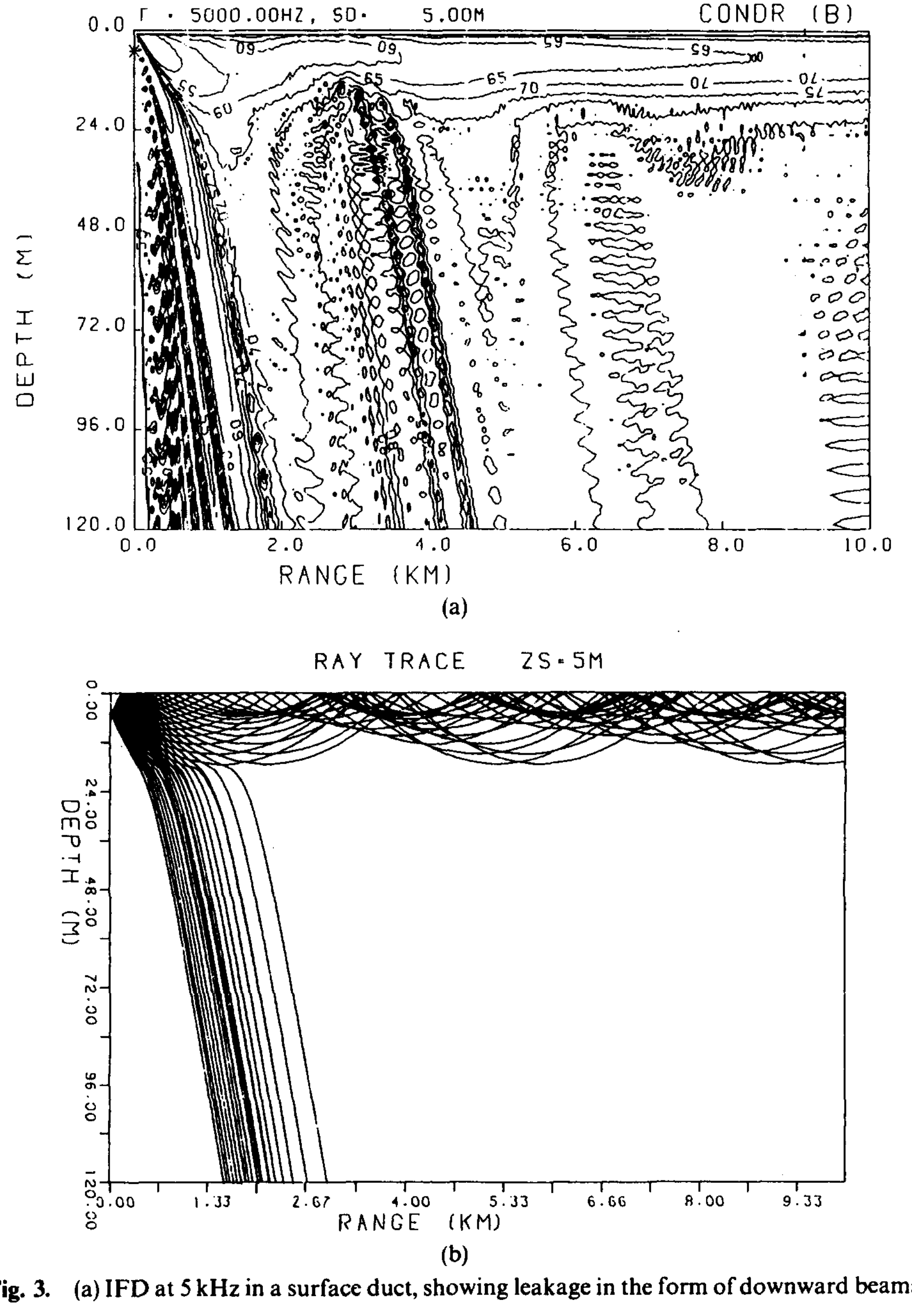

Fig. 3. (a) IFD at 5 kHz in a surface duct, showing leakage in the form of downward beams emerging at every cycle. (b) Corresponding ray trace.

plot) for a surface duct. There are strong similarities in the shadow zone boundaries, but the sharp-edged shadow envisaged by ray exponents is clearly a myth. This area is partially covered by duct leakage which clearly includes downward-propagating beams repeating at the cycle distance and emerging from the duct just before the ray turning points at ranges of 1·3, 4·6 and 7·6 km.

4.2 SNAP and SUPERSNAP

Normal-mode models are relatively robust, and they have the potential advantage of being able to calculate intensity at any range or depth without making computations at all intermediate ranges. Computation time consists of the 'overhead' of calculating the modes, which increases in proportion to the number of depth points, the number of modes and the uncertain but usually small number of iterations, and then the mode summation for each chosen range and depth point.

For most purposes the discrete mode sum is adequate. However, there are several weaknesses in deep water apart from the large number of modes and the convergence problems already mentioned. As a further extension of the analogy with the violin string which was introduced in section 3.3, a normal mode is a vertical standing wave caused by upward- and downward-going waves interfering. The amplitudes of the two waves need to be comparable to form a true standing wave, and this cannot be so until there have been at least a few reflections or refractions to turn the down-going rays around. Therefore the normal mode solution is incomplete for ranges shorter than the cycle distance[98] for each mode (or ray family).

There are a number of other important effects that cannot be handled by discrete normal mode models, essentially because the effects require lossy modes to be included. Lossy modes form a continuous, rather than discrete spectrum, and this requires evaluation of a branch line integral as well as the sum. An important return at low frequencies in deep water at ranges before the first bottom-refracted arrival is bottom reflection. Reflections from a density discontinuity where velocity is more or less continuous are necessarily lossy because the Rayleigh reflection coefficient is a constant independent of angle, and there is no critical angle. The reflections therefore do not feature in the usual mode sum. Nevertheless, these reflections may be quite significant, as seen in the comparison of SUPERSNAP with SAFARI (Fig. 4). This example has a water depth of about 1000 m. At ranges beyond about 10 km there are many deep bottom-refracted paths, and the good agreement implies that a discrete sum is perfectly adequate. At shorter ranges SAFARI shows many rapidly interfering bottom reflections which are not seen in SUPERSNAP.

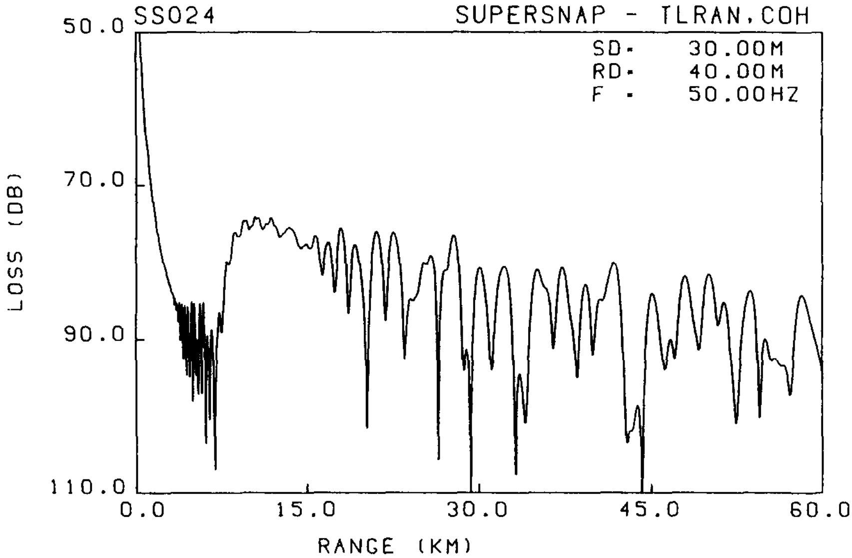

(a)

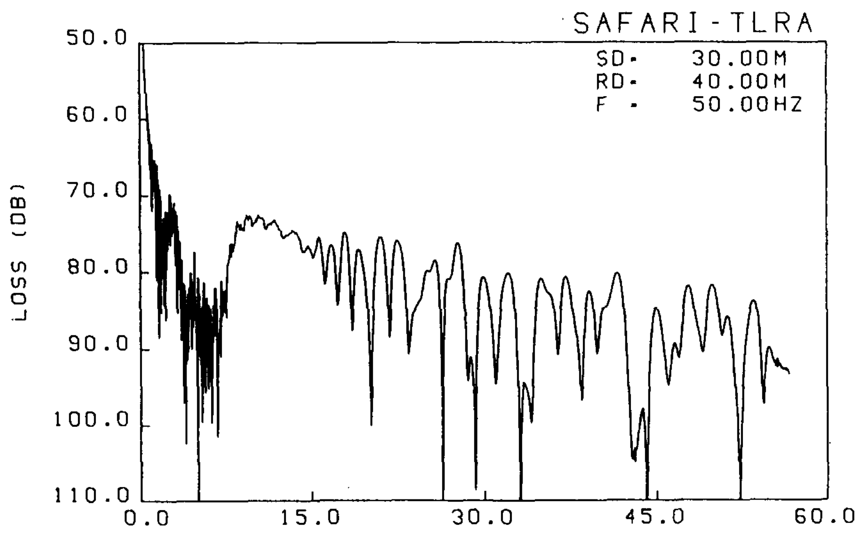

(b)

Fig. 4. (a) SUPERSNAP and (b) SAFARI showing the neglected short-range reflections due to density differences at the sea bed.

Shear effects have been included in normal mode models,[67] but in many environments of interest lossy modes are again important, and these can be handled more faithfully by SAFARI. For instance, the shear critical angle is always smaller than the compression critical angle (since shear speed is less than compression speed) so that the spectrum includes a set of decaying modes, which is neglected by the discrete sum, but which may nonetheless be significant.

The adiabatic approximation can be used for 'slowly varying' environments, but it is sometimes difficult to see what this means in any other way than the statement that there is no mode coupling. In discussing applications of ray invariants, the author of Ref. 21 looked at the equivalence between adiabatic modes and ray angles and their joint conditions for validity in a reflecting duct. Rays become steeper in shallow water in a *reversible* way, provided that the reflecting surfaces are smooth and their shapes change slowly. This is equivalent to the adiabatic approximation. It is clear that in crossing a ridge, say, the process is not reversible if the critical angle is passed at any stage; it is also clear that undulations in between bottom bounces will produce a virtually random additional angle to the ray. Therefore the condition is roughly that ray angles (at the sea bed) should always be considerably greater than the slope of the sea bed, so that there are many bounces within a small change of environment.

4.3 SAFARI

SAFARI is an exact solution of the Helmholtz equation (in a stratified medium) for ranges greater that a wavelength or so. Compression and shear velocities with separate absorptions and stepped density profiles can be handled. Limitations are not fundamental since they stem from the problem of resolution in wavenumber which can be alleviated (without changing the code) given enough computation time and numerical accuracy.

The number of points in the Fourier transform, N, constrains the range, r_F, and the usable portion of this is $r_u = \frac{1}{2} r_F$. The usual Fourier transform relation is

$$2\pi N = \Delta K r_F \qquad N = \frac{f r_F}{c_1}\left(1 - \frac{c_1}{c_2}\right) \tag{16, 17}$$

where ΔK, f, c_1 and c_2 are, respectively, the wavenumber resolution, frequency, and lower and upper phase velocity assumed in calculating the Green's function (as a function of horizontal wavenumber K). The CPU time to carry out the FFT is relatively small, but calculation of the N Green's function values for entry into the FFT increases in proportion to N. Calculations become much more efficient for large numbers of receivers,[10] because the Green's function has been matched at all the layer boundaries and its form is known in each layer so that it is easily evaluated anywhere without starting from scratch. Without increasing N the only way of improving the resolution in deep water where there is a large number of loss-free modes (each corresponding to a spike in wavenumber, i.e. a pole in the complex wavenumber plane) is to offset the line of integration from the real wavenumber axis by adding a small imaginary part to K. This has the effect of moving the integration line further from the poles (which are on or very close to the real axis) so that the integral appears smoother; consequently resolution with the same N is improved. A criterion has been given[48] for the offset which can be written in terms of dB per wavelength, J, as

$$J = 60c_1/fr_F \tag{18}$$

Substituting for the maximum range this reduces to

$$J = 60\frac{c_1}{N}\left(\frac{1}{c_1} - \frac{1}{c_2}\right) \simeq \frac{60}{N}\left(1 - \frac{c_1}{c_2}\right) \tag{19}$$

A rule of thumb for having achieved a well sampled K-plot is that the function should look like a modulated sine wave with a smooth envelope. This is nearly always true for low K, but for high K a jagged envelope demonstrates poor sampling.

This effect and the consequences for transmission loss are shown in Figs 5(a)–(f). Firstly a small offset results in jagged peaks (a) and a 'noisy' transmission loss plot (b). The optimum offset case (c) shows a much neater K-plot with a smooth envelope and the low order modes have been lumped together. The loss plot (d) is relatively smooth but still rather noisy at long range. A large offset results in a very smooth K-plot (e), but the penalty is that the intensity begins to increase with range (f). In effect, the artificial insertion of a small imaginary part to the wavenumber ε damps the modal resonances, but to retain the low loss of the original modes the formal mathematics[48] needs to compensate by amplifying the result by an exponential exp (εr) at each range r. This delicate balance is upset if ε becomes too large.

A complementary point is that the Green's function amplitude must tail off to zero for high and low K to avoid superimposing Fourier transform noise. This appears at first sight to be a reasonable approximation in the first case, but as the function broadens with increasing offset the left-hand side rises (relatively) so as to be appreciably 'chopped' by the end of the Fourier transform. In fact, what has happened is that the area under the left-hand side has remained constant and so has the area under the right-hand side (low order modes), but the original spikiness of the modes gave the mistaken impression that the low K Green's function amplitude was negligible.

The earlier equation for N makes it clear that for fixed computation time

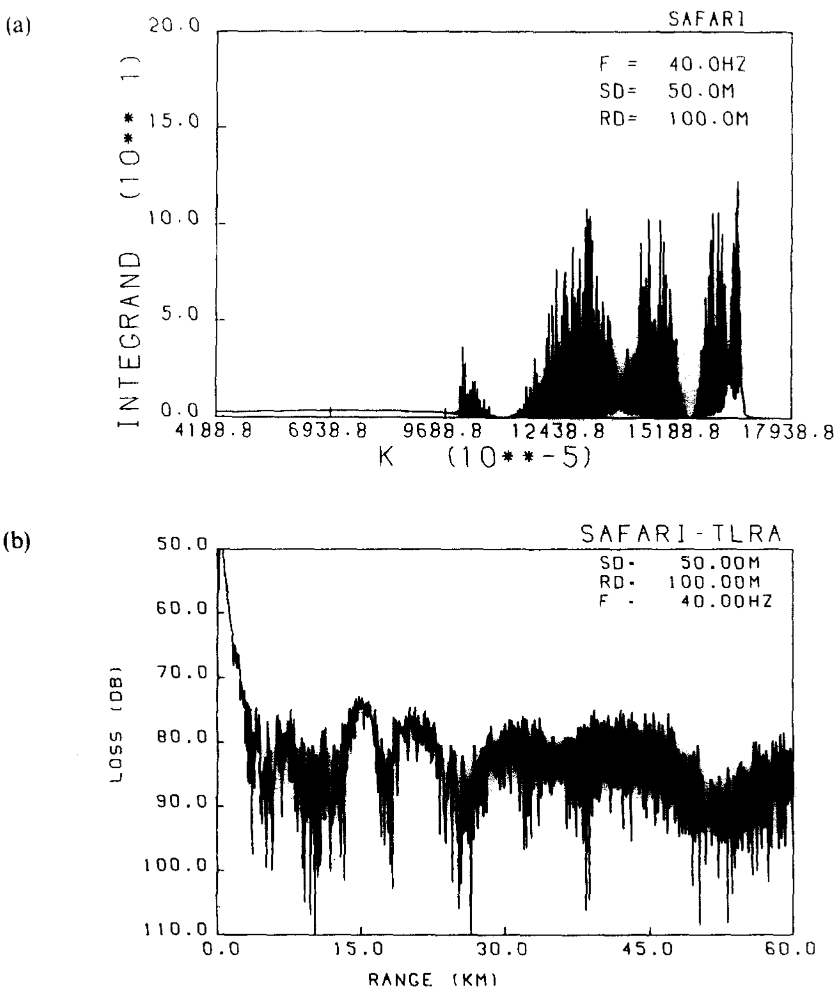

Fig. 5. The effect of altering the integration line offset from the real K-axis: (a), (b) small offset; (c), (d) optimum offset; (e), (f) large offset.

(i.e. fixed N) the user may trade range for velocity contrast or frequency. At a fixed frequency this usually means that he or she has to open up the phase velocity limits c_1 and c_2 to accommodate the real environment. This puts a restriction on the maximum range. When there is an abrupt density change at the sea bed the wavenumber plot (integrand) often has significant amplitudes for phase velocities well above the maximum velocity in the sediment (i.e. wavenumbers much lower than $2\pi f/c_B$), and a suitable phase velocity must either be found by trial and error or set to infinity.

An interesting check for SAFARI in a non-trivial environment is given by an analytical image calculation. Imagining source images in the multiple surface and bottom image planes at depths $\pm 2nH \pm z_s$ one can group the

(c)

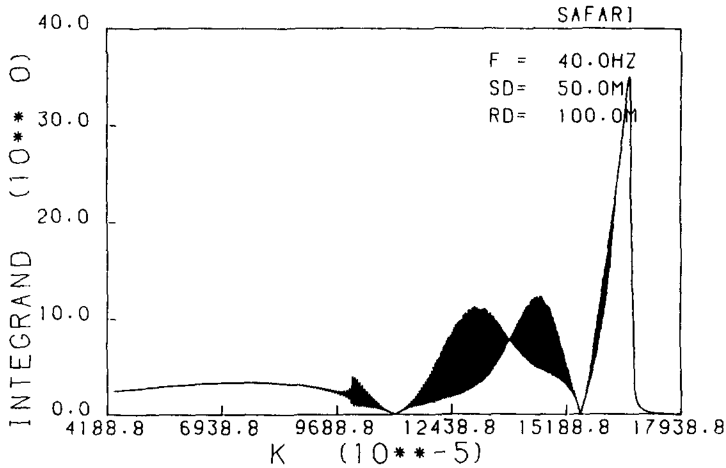

(d)

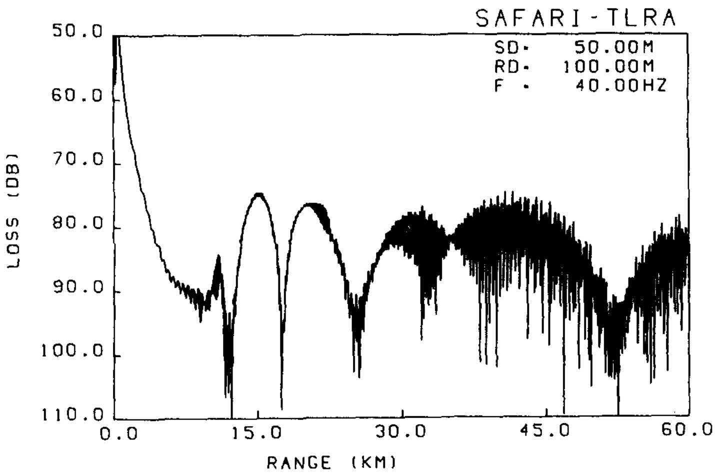

Fig. 5.—*contd.*

sources according to the number of bottom interactions (in isovelocity water). The true source and one image (in the surface) have no bottom interactions and produce a Lloyd's mirror effect. The next four images (or four rays) have one bottom interaction (but different numbers of surface interactions). The next four have two bottom interactions, and so on. It is assumed that the angle differences between each order of reflection will be so great that very rapid oscillations will result, but that they can be neglected because usually one order of reflection dominates for most ranges. Thus the main point of interest is the remaining relatively slow beats in the spatial pattern. The transmission loss for each reflection order is easily shown to be

$$TL = -10 \log P$$

$$P = 16(R^n/r')^2 [\sin^2(a_r)\sin^2(a_s) + \sin^2(a_{sr})(1 - \sin^2(a_r) - \sin^2(a_s))] \quad (20)$$

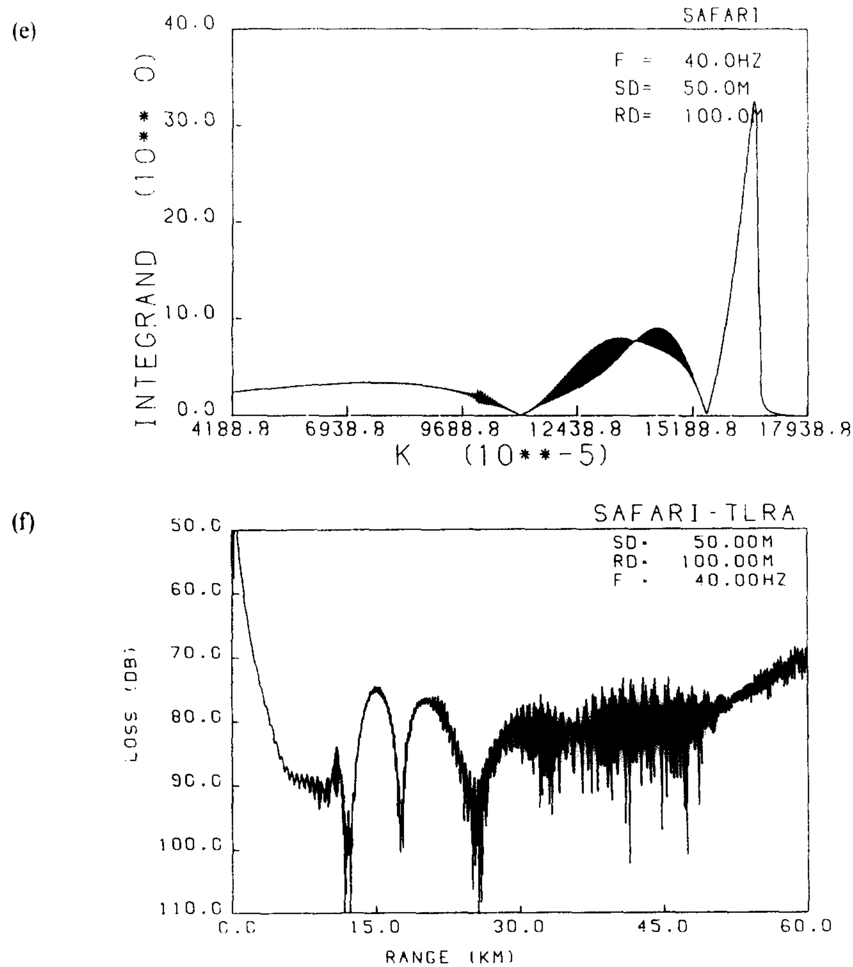

Fig. 5.—*contd.*

for $n \geq 1$, where

$$\begin{aligned} r'^2 &= (2nH)^2 + r^2 \\ a_r &= 2knHz_r/r' \\ a_s &= 2knHz_s/r' \\ a_{sr} &= kz_s z_r/r' \end{aligned} \tag{21}$$

If the bottom interface is marked only by a change in density ρ, the Rayleigh reflection coefficient is

$$R = (\rho - 1)/(\rho + 1) \tag{22}$$

This is a constant for all angles, and Fig. 6 compares numerical evaluation of eqn (20) for $n = 1$ and 2 and Lloyd's mirror with SAFARI in the case where $R = 0{\cdot}1$. Agreement is extremely good, and the residual interference

(a)

(b)

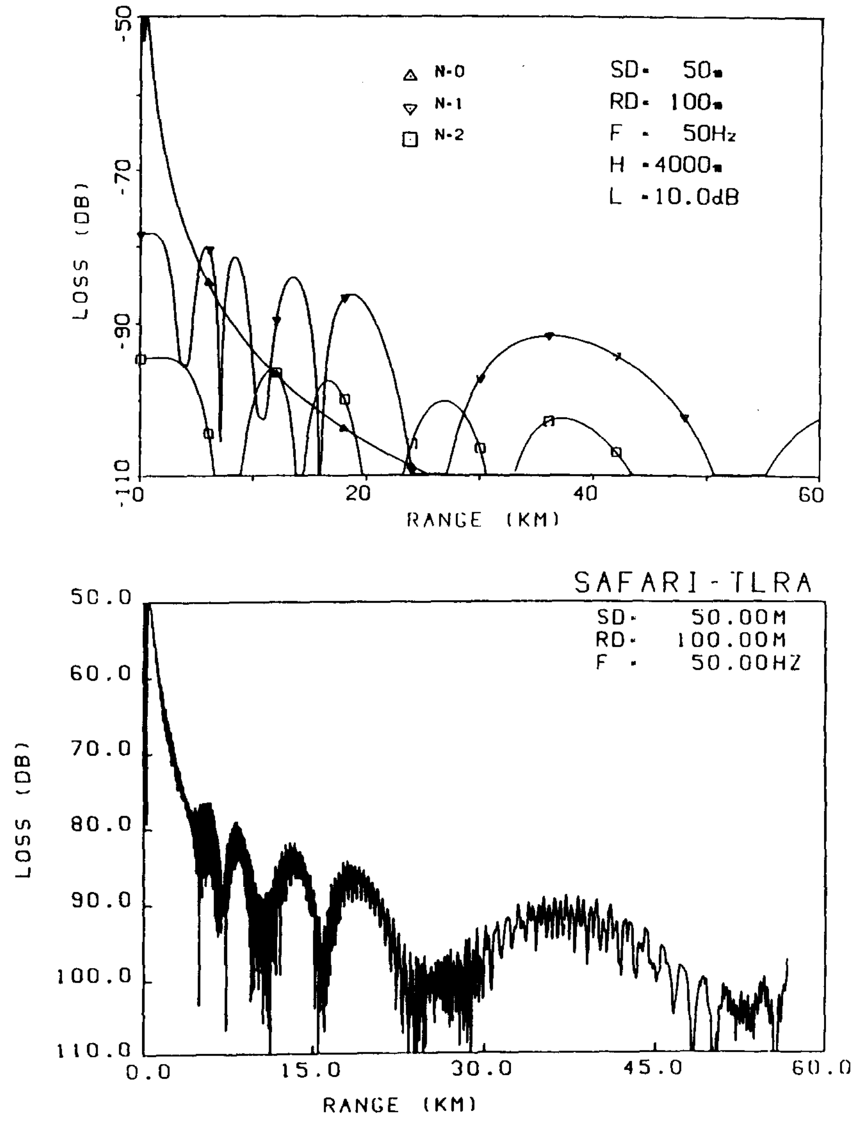

Fig. 6. An image calculation (a) used as a diagnostic tool to compare with SAFARI (b).

can at least partly be accounted for by the neglected beating between paths with different numbers of bottom reflections. Other examples have shown that the image calculation is extremely useful for filling in the short range reflections which are omitted by other models.

4.4 PAREQ and IFD

There is a considerable literature on the parabolic equation and its shortcomings.[81,99–102] The PE has a fundamental elevation angle

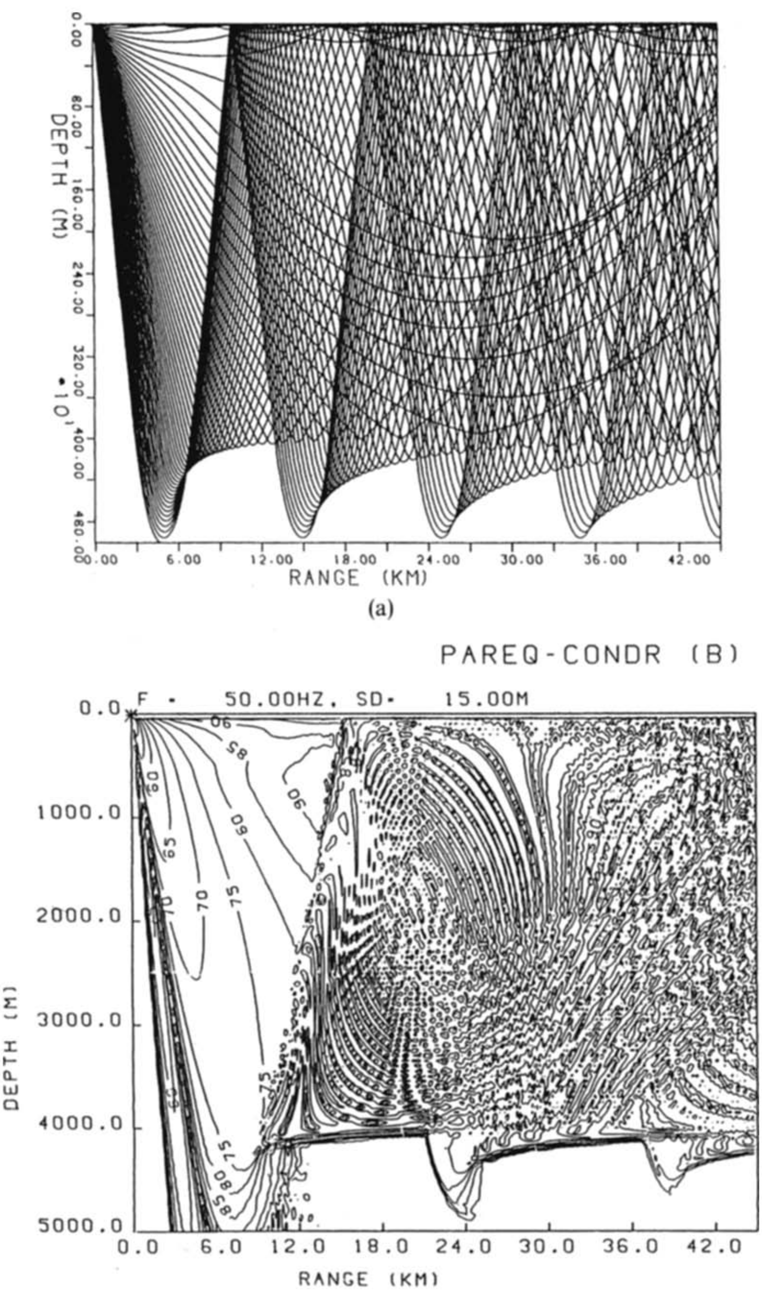

Fig. 7. Angle or phase errors in the parabolic equation, illustrated by the discrepancies in range to the first bottom refracted arrival at the sea surface. (a) GRASS ray trace; (b) PAREQ.

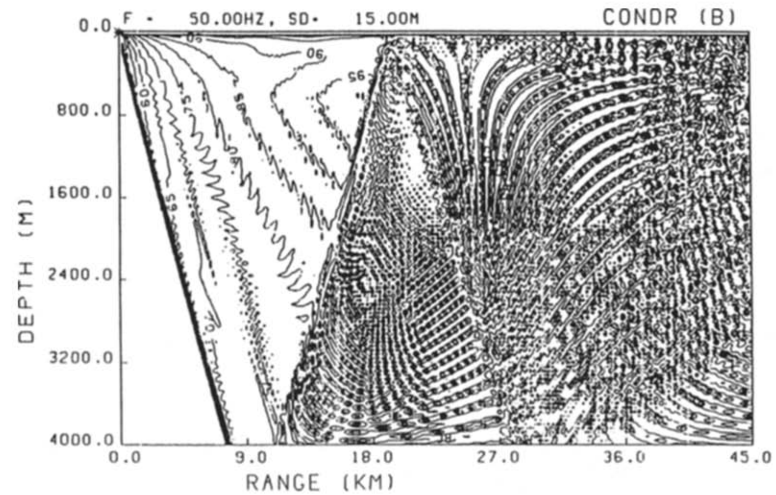

(c)

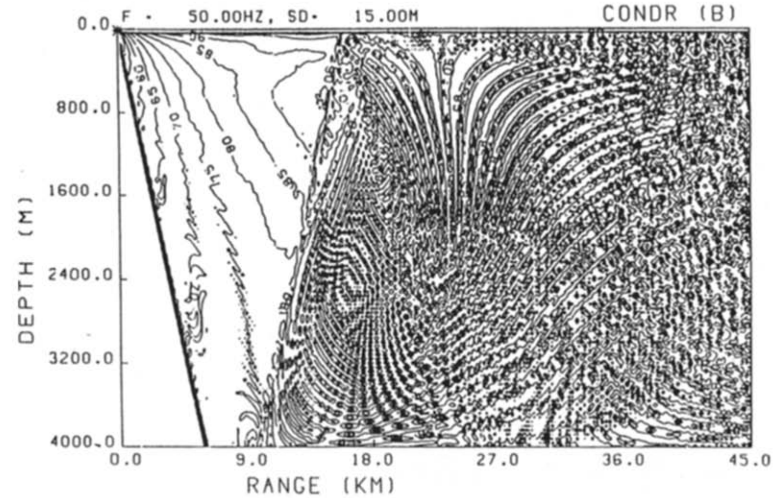

(d)

Fig. 7.—*contd.* (c) IFD (N); (d) IFD (W). A strongly refracting sediment layer between 4000 and 5000 m, is assumed.

restriction regardless of its implementation because it is an approximation to the Helmholtz equation. IFD has two implementations,[56] one due to Tappert[53] (narrow angle) and one due to Claerbout[103] (wide angle), referred to here as IFD (N) and IFD (W). PAREQ and IFD (N) are often quoted as having a limit of order 20°, whereas IFD (W) has a limit of 40°. A weakness in these models is that there is no sudden change in the output at these angles, and contour and loss plots continue to look realistic to the uninitiated. This is because the wide angle returns are effectively mapped into narrow angles rather than being ignored.[104] An environment with a sediment velocity of 1600 m/s and low absorption is all that is required to produce 20° rays. After a long enough range the steep rays will die out, of course, but at low frequencies there are often significant returns remaining within the first convergence zone range.

A ray trace in which rays are transmitted through the sea bed at 4000 m and refracted from the sediment back to the water is shown in Fig. 7(a). A repeated pattern of rays penetrating to the bottom of the sediment (5000 m) is seen. At 50 Hz, where the wavelength is 30 m, this plot is reasonably representative except that it says nothing about the intensity. Equivalent intensity contour plots for PAREQ, IFD (N) and IFD (W) are shown in Figs 7(b), (c) and (d). Since the loss is quite low (0·15 dB/wavelength) the repeated pattern still exists in each case. What is striking is the varying distances to the first bottom-refracted arrival at the surface; these are 10, 16, 21 and 16 km respectively. The grazing angle of the rays at the sea bed is 54° (with a sediment velocity gradient of 1 m/s/m) so it is not surprising that it is difficult to predict performance once the rough angle limit has been exceeded. Thomson & Wood[104] have suggested a practical method for realising De Santo's correction.[27] This consists of separating out each horizontal wavenumber component by Fourier transforming in range and performing a weighting and mapping to a new wavenumber before transforming back to range. In effect, the large-angle components are separately set to larger angles while the small-angle components are left untouched. An alternative approach is taken by Tolstoy,[92] where a similar effect is achieved by altering the velocity profile progressively away from the velocity minimum. Provided that the velocity contrast is small it is possible to make corrections by choosing the reference sound speed carefully; a 'natural' choice is described in Ref. 105. Using the WKB approach this can be converted into a very simple practical formula.[106]

There is an additional effect (which may be seen in Figs 7(b), (c) and (d) at very short ranges when source and receiver are at different depths. The marching solution results in zero intensity for $|z_s - z_r| > r \tan \alpha$, where α is a constant angle depending on the algorithm and the range step length.

The standard versions of IFD and PAREQ cannot handle density changes in the sediment exactly. Instead PAREQ, for instance, emulates the change by altering the velocity profile. However, it can easily be seen that a boundary with a density discontinuity but continuous velocity gives a constant reflection coefficient, independent of angle. Thus at short range there will be many reflections at steep angles right up to 90°. This can only be emulated if the two velocities are close in value and consequently the reflection coefficient is very low. More rigorous work on inclusion of density has been done by St Mary.[80]

A practical limitation to the PE is the cost of computation time. This rises in proportion to the number of calculation points in depth and range. The usual step sizes of $\lambda/4$ and $\lambda/2$ result in computation time being proportional to f^2. However, this is offset to a certain extent by the fact that the calculation necessarily includes many receiver depths and is therefore directly suitable for contouring. In the vertical there is, in principle, some scope for increasing the step sizes since the spatial variation cannot be more rapid than the vertical wavelength of the highest order mode (at least for calculations starting beyond the cycle distance). Experimenting with step size is often made difficult by the assumption elsewhere in the code (e.g. in the Gaussian initialisation) that the step size is no greater than a quarter of a wavelength.

5 REGIONS OF APPLICABILITY

Each model has a range of input parameters for which the model outputs are reliable. There are two independent questions that need to be answered in any application. One is, what are these limits for a particular model? The other is, what are the required values of the inputs for the environment in question? These 'fuzzy' areas may not overlap, and there may even be areas where no model works. The input parameters of all models break down into operational parameters (i.e. frequency, source depth, receiver depth and range), environmental parameters (i.e. velocity profile, water depth, sediment depth, absorption and velocity and their gradients in the sediment, density etc.) and numerical tuning factors (e.g. reference sound speed, depth and range increments in IFD; integration offset, velocity contrast versus FFT size trade-off in SAFARI; and range and angle increments in GRASS).

5.1 Effective angles dictated by the environment

A clearer picture of the conditions under which the model has to operate is necessary in order to proceed further, and this can be seen by attempting to limit the number of parameters. The approach here is to take only three parameters: range and frequency, with the (horizontally stratified) environment drastically reduced to one parameter. These parameters define a volume that must be covered by the model.

The single parameter used to describe the environment is the 'effective angle', as described below. At a particular range the total energy from an omnidirectional source is spread into a range of angles; Snell's law and the reflection coefficients dictate the relation between angle and the complete velocity and density profile, but attenuation effects will eventually narrow the angle down at long range. The range of angles is related to the number of remaining modes that have non-zero amplitudes at source and receiver depth (as can be seen from the WKB solution) and is related to Weston's invariants and flux formulation[26] which are useful concepts for range-dependent media.

The initial energy split between surface duct, water column and sediment is determined by the angle at the source for the limiting ray in each duct, i.e.

$$\theta = \cos^{-1}(c_s/c) \tag{23}$$

where c_s is the velocity at the source and c corresponds to the maximum velocity in either the surface duct, the water column or the entire profile including the sediment. From simple flux arguments or WKB-mode formulae the distribution of energy in the ducts is in the proportions

$$\frac{\theta_d}{H_d} : \frac{(\theta_w - \theta_d)}{H_w} : \frac{(\theta_b - \theta_w)}{(H_b + H_w)}$$

where the subscripts refer to the surface duct (d), water column (w) and sediment (b), and H is the appropriate layer thickness.

The 'effective angle' is defined, rather loosely, as the steepest angle that succeeds in making a significant contribution for the given source–receiver combination at the given range. It is especially useful in defining the acoustic effects of the environment because it can be compared directly with angle limits of models or translated into wavenumber limits as appropriate. There are, of course, many complications, particularly at low frequency, such as near-boundary effects, which need to be borne in mind as well.

At a single frequency there is a curve in the r–θ plane which defines the angles θ_{eff} that must be catered for at each range. Examples are shown in Figs 8(a) and (b) for low and high frequency respectively. The region that must be covered is above and to the left of the curve, i.e. for a given range r, all $0 < |\theta| < \theta_{\text{eff}}(r)$.

With a dense sediment there will be reflections at angles up to 90°, but at extremely short range these will be overpowered by the direct path. The effective angle will therefore be smaller than 90° depending on the detailed geometry, but steep angles will become significant at ranges comparable with the water depth. From then on the effective angle will fall to the critical angle and level out after a range of about the cycle distance[98] ($2H \cot \theta_c$). If the energy is spread more or less uniformly in angle each contribution will drop out at a range where its total loss, RL, exceeds a certain level. The relation between RL and range r is easily calculated by considering the absorption in transitting the sediment, and for small grazing angles, θ,

$$RL = rf\alpha\theta^2/Hc' \tag{24}$$

where f, α, H and c' are frequency, absorption in dB per wavelength, water

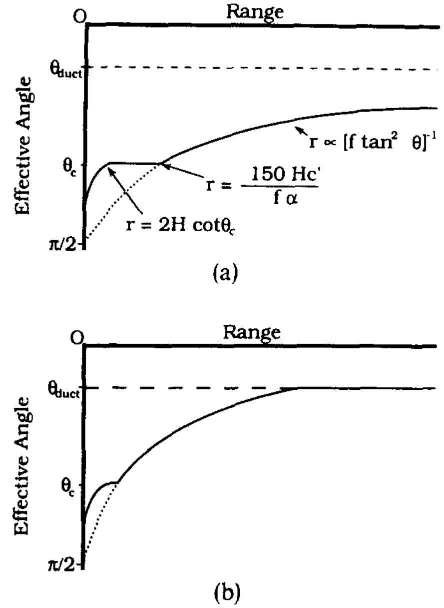

Fig. 8. The regime defined by the environment in terms of a single parameter, the 'effective angle', versus range for (a) low and (b) high frequencies.

depth and velocity gradient in the sediment respectively. If the drop-out level is taken as a constant for all contributions then the range is

$$r \propto Hc'/f\alpha\theta^2 \tag{25}$$

and has already been calculated for mode stripping.[107] If there is a surface duct (above cut-off) the effective angle reduces finally to a value defined by the velocity contrast and depth of the duct.

Naturally, energy partitioning between surface duct, water column and sediment-refracted arrival must also be considered. At low frequencies where the surface duct cannot support any modes its energy contribution is zero so that the surface duct can be ignored. At higher frequencies, despite the low spread of angles, there may be relatively high energy density in the duct because of its limited depth. In extreme circumstances this may make it possible to ignore the bottom returns despite their high angles. It is difficult to invent a general rule, though, because the relative strengths of the various returns change in an arbitrary manner. The best way to find out is to perform a pilot run to see which returns dominate and where, and then to use a ray trace to estimate the appropriate angles.

5.2 Angles covered by GRASS

GRASS can be run in two ways, one having a reflection loss table strictly covering reflections and ignoring bottom-refracted paths, and the other

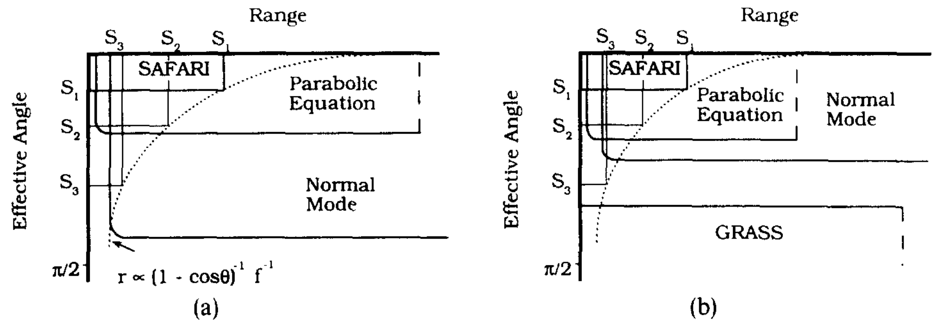

Fig. 9. The areas of coverage given by GRASS (ray), normal-mode parabolic equation and SAFARI models for (a) low and (b) high frequencies.

having a compromise table covering all upward-turning rays. Neither case features in the low-frequency graph, Fig. 9(a), but the latter case occupies the whole of the high-frequency graph, the only limitation being the practical consideration of computation time and accuracy at the right-hand edge. The strict reflection loss case which is shown in Fig. 9(b) is only valid for the case in which bottom-reflected paths (total loss $RL = rL\theta/2H$) are stronger than refracted paths (eqn (24)). This condition is

$$\theta \gg c'L/2f\alpha \tag{26}$$

5.3 Angles covered by SNAP and SUPERSNAP

The discrete normal-mode solution is valid at ranges beyond the cycle distance and frequencies above the cut-off of the entire water–sediment column. Shooting methods such as SNAP suffer not only from excessive computation time when there are many modes but also from difficulties with convergence in the mode shapes (particularly low-order modes). Thus they run into difficulties at high frequencies, but may also have trouble in deep water at low frequencies. The convergence problems are alleviated by SUPERSNAP although computation time will still limit performance. There is no particular angle limit in the normal-mode approach (other than, by definition, the critical angle) but, for a fixed computation time, frequency could be increased by artificially restricting the number of modes (in principle, the restriction could be to any given set, not necessarily the lowest order modes). This is shown by the horizontal line in Fig. 9.

5.4 Angles covered by SAFARI

The coverage given by SAFARI cannot be shown once and for all in Fig. 9, since there is a choice to be made by the user between range and velocity contrast (effective angle). The computation time is roughly proportional to the number of points in the FFT, N and, putting $\cos\theta_{\text{eff}} = c_1/c_2$, the earlier formula (eqn (17)) corresponds to

$$CPU \propto N \qquad N = fc_1^{-1} r_F (1 - \cos\theta_{\text{eff}}) \tag{27}$$

For fixed CPU the $\theta_{\text{eff}}(r)$ curve is therefore

$$\theta_{\text{eff}} = \cos^{-1}[1 - Nc_1/fr_F] \tag{28}$$

This is shown by the dotted line in Fig. 9. The user can choose any point on this dotted line to define θ_{eff} and r_F, and so he has a choice of the rectangular boxes of validity defined by S_1, S_2, S_3 etc. However, he does not have a free hand because the answers will be incorrect or suspect if the effective angle in Fig. 9 does not cover the required angle shown in Fig. 8, so there is always a limit on range.

A possible, although tedious, way of extending the range of SAFARI is to calculate loss for short extensions in range from non-zero starting points in a piecewise fashion. Another way is to calculate short-range TL from a high velocity contrast run, and then calculate long-range TL from a separate low velocity contrast run. The overlap is usually well behaved.

5.5 Angles covered by PAREQ and IFD

The parabolic equation is valid for large ranges and angles below some limit for the implementation regardless of frequency. The effect is a flat but hazy cut-off, as shown by the solid line in Fig. 9. At short ranges there may be phase errors, and at very short ranges there are guaranteed angle violations unless the receiver is at the same depth as the source. The practical limitation of computation time (and ultimately numerical accuracy) is shown by the dotted line on the right.

5.6 General comments on coverage

At short range the only wave treatment to give reliable coverage is SAFARI. This is complemented by and overlaps with SUPERSNAP at longer ranges. At frequencies where SAFARI becomes too expensive to run there is no other model that can handle short-range returns, and simple image calculations may be able to fill the gap. In a strongly range-dependent environment where neither SAFARI nor SUPERSNAP is applicable there is a strong possibility of a hole in coverage at high frequencies, which becomes a certainty at low frequencies. One hopes that, in practice, the environment only requires small angles that either GRASS or PE can handle.

6 CONCLUSIONS

A review of four types of propagation model has been given including GRASS (rays), SNAP and SUPERSNAP (normal mode), SAFARI and FFP (Green's function), and PAREQ and IFD (parabolic equation). References have been made to various model comparisons. Brief descriptions of the models and the environments to which they apply have led to a discussion of their limitations in terms of validity, computation time and tuning. Finally, an attempt has been made to map out regions of applicability and to present a way of choosing models in practice.

ACKNOWLEDGEMENT

A substantial part of the work on which this review is based was carried out under contract to the Admiralty Research Establishment (UK).

REFERENCES

1. Urick, R. J., *Principles of Underwater Sound.* McGraw-Hill, New York, 1967.
2. Tolstoy, I. & Clay, C. S., *Ocean Acoustics: Theory and Experiment in Underwater Sound.* McGraw-Hill, New York, 1966.
3. Clay, C. S. & Medwin, H., *Acoustical Oceanography.* John Wiley, New York, 1977.
4. Officer, C. B., *Introduction to the Theory of Sound Transmission.* McGraw-Hill, New York, 1958.
5. Kinsler, L. E., Frey, A. R., Coppens, A. B. & Sanders, J. V., *Fundamentals of Acoustics.* John Wiley, New York, 1982.
6. Weinstein, M. S. & Henney, A. G., Wave solution for air-to-water sound transmission. *J. Acoust. Soc. Am.*, **37** (1965) 899–901.
7. Urick, R. J., Noise signature of aircraft in level flight over a hydrophone in the sea. *J. Acoust. Soc. Am.*, **52** (1972) 993–9.
8. Chapman, D. M. F., The effects of seabed interaction on air-to-water sound transmissions. *J. Acoust. Soc. Am.* **82** Suppl. 1 (1987) DDD2.
9. Harrison, C. H., Propagation in air using SAFARI (unpublished).
10. Schmidt, H., Modelling of pulse propagation in layered media using a new fast field program. In *Hybrid Formulation of Wave Propagation and Scattering*, ed. L. B. Felsen. Martinus Nijhoff, Dordrecht, 1984, pp. 337–56.
11. Meeks, M. L., *Radar Propagation at Low Altitudes.* Artech House, MA, 1982.
12. Hamilton, E. L., Geoacoustic modeling of the sea floor. *J. Acoust. Soc. Am.*, **68** (1980) 1313–40.
13. Rauch, D., Experimental and theoretical studies of seismic interface waves in coastal waters. In *Bottom Interacting Ocean Acoustics*, ed. W. A. Kuperman & F. B. Jensen. Plenum Press, New York, 1980, pp. 307–27.
14. Crowther, P. A., Acoustical scattering from near surface bubble layers. In

Cavitation and Inhomogeneities in Underwater Acoustics, ed. W. Lauterborn. Springer-Verlag, Berlin, 1980, pp. 194–204.
15. Arctic acoustics. *J. Acoust. Soc. Am.*, **82**, Suppl. 1 (1987) C,M.
16. Under-ice propagation. *J. Acoust. Soc. Am.*, **80**, Suppl. 1 (1986) Y.
17. Kuperman, W. A., Porter, M. B. & Perkins, J. S., Three-dimensional oceanographic acoustic modeling of complex environments. *J. Acoust. Soc. Am.*, **82**, Suppl. 1 (1987) S1.
18. Weston, D. E., Horizontal refraction in a three dimensional medium of variable stratification. *Proc. Phys. Soc. Lond.*, **78** (1961) 46–52.
19. Weston, D. E. Guided propagation in a slowly varying medium. *Proc. Phys. Soc. Lond.*, **73** (1959) 365–84.
20. Harrison, C. H. Three-dimensional ray paths in basins, troughs and near seamounts by use of ray invariants. *J. Acoust. Soc. Am.*, **62** (1977) 1382–8.
21. Harrison, C. H., Acoustic shadow zones in the horizontal plane. *J. Acoust. Soc. Am.*, **65** (1979) 56–61.
22. Buckingham, M. J., Theory of three-dimensional acoustic propagation in a wedgelike ocean with a penetrable bottom. *J. Acoust. Soc. Am.*, **82** (1987) 198–210.
23. Buckingham, M. J., Theory of acoustic propagation around a conical seamount. *J. Acoust. Soc. Am.*, **80** (1986) 265–77.
24. Glegg, S. A. L. & Yoon, J. R., Range-dependent cut-on frequency in a three-dimensional ocean environment. *J. Acoust. Soc. Am.*, Suppl. 1, **82** (1987) CC1.
25. Siegmann, W. L., Kriegsmann, G. A. & Lee, D., A wide-angle three-dimensional parabolic wave-equation. *J. Acoust. Soc. Am.*, **78** (1985) 659–64.
26. Weston, D. E., Rays, modes and flux. In *Hybrid Formulation of Wave Propagation and Scattering*, ed. L. B. Felsen. Martinus Nijhoff, Dordrecht, 1984, pp. 47–60.
27. De Santo, J. A. *Ocean Acoustics*. Springer-Verlag, New York, 1979.
28. Jensen, F. B., Numerical models in underwater acoustics. In *Hybrid Formulation of Wave Propagation and Scattering*, ed. L. B. Felsen. Martinus Nijhoff, Dordrecht, 1984, pp. 295–335.
29. Gilbert, K. E., Evans, R. B., Chin-Bing, S. A., White, D., & Kuperman, W. A., Some new models for sound propagation in bottom-limited ocean environments. In *Acoustics and the Sea Bed*, ed. N. Pace. Bath University Press, UK, 1983, pp. 243–50.
30. Evans, R. B., A coupled mode solution for acoustic propagation in a waveguide with stepwise depth variations of a penetrable bottom. *J. Acoust. Soc. Am.*, **74** (1983) 188–95.
31. Rutherford, S. R. & Hawker, K. E., Consistent coupled mode theory of sound propagation for a class of nonseparable problems. *J. Acoust. Soc. Am.*, **70** (1981) 554–64.
32. Pierce, A. D. Extension of the method of normal modes to sound propagation in an almost-stratified medium. *J. Acoust. Soc. Am.*, **37** (1965) 19–27.
33. Milder, D. M., Ray and wave invariants for SOFAR channel propagation. *J. Acoust. Soc. Am.*, **46** (1969) 1259–63.
34. Kalinowski, A. J., Survey of finite element related techniques as applied to acoustic propagation in the ocean—1. Finite element method and related techniques. *Shock and Vibration Digest*, **11** (1979) 9–16.
35. Murphy, J. E. & Chin-Bing, S. A., The finite element method applied to ocean acoustic propagation. *J. Acoust. Soc. Am.*, **81**, Suppl. 1 (1987) D1.

36. Marsh, H. W. & Schulkin, M., Shallow water transmission. *J. Acoust. Soc. Am.*, **34** (1962) 863.
37. Lindop, P. M., The deduction of approximate values of sediment depth from propagation loss measurements. In *Ocean Seismo-Acoustics*, ed. T. Akal & J. M. Berkson. Plenum Press, New York, 1986, pp. 243–52.
38. Harrison, C. H. & Cousins, P. L., A study of propagation loss dependence on sediment layer thickness using the fast field program. In *Ocean Seismo-Acoustics*, ed. T. Akal & J. M. Berkson. Plenum Press, New York, 1986, pp. 139–48.
39. Urick, R. J. *Sound propagation in the sea.* Peninsula Publishing, Los Altos, 1982.
40. Etter, P. C., Underwater acoustic modelling techniques. *Shock and Vibration Digest*, **13** (1981) 11–20.
41. Etter, P. C., Underwater acoustic modelling techniques. *Shock and Vibration Digest*, **16** (1984) 17–23.
42. Etter, P. C., Numerical modelling techniques in underwater acoustics. *J. Acoust. Soc. Am.*, **82**, Suppl. 1 (1987) UU1.
43. Cornyn, J. J., GRASS: a digital-computer ray-tracing and transmission-loss-prediction system. Volume I—overall description. Nav. Res. Lab., Report No. 7621, 1973.
44. Cornyn, J. J., GRASS: a digital-computer ray-tracing and transmission-loss-prediction system. Volume II—user's manual. Nav. Res. Lab., Report No. 7642, 1973.
45. Bartburger, C. L., PLRAY—a ray propagation loss program. Nav. Air. Dev. Center, Report No. NADC-77296-30, 1978.
46. Jensen, F. B. & Ferla, M. C., SNAP: The SACLANTCEN normal-mode acoustic propagation model. SACLANT Memo SM-121, 1979.
47. Porter, M. & Reiss, E. L., A numerical method for ocean-acoustic normal modes. *J. Acoust. Soc. Am.*, **76** (1984) 244–52.
48. Schmidt, H., *SAFARI User's Guide.* SACLANT ASW Research Centre, La Spezia, Italy, 1987.
49. Schmidt, H. & Jensen, F. B., A full wave solution for propagation in multilayered viscoelastic media with application to Gaussian beam reflection and fluid–solid interfaces. *J. Acoust. Soc. Am.*, **77** (1985) 813–25.
50. Schmidt, H. & Glattetre, J., A fast field model for three-dimensional wave propagation in stratified environments based on the global matrix method. *J. Acoust. Soc. Am.*, **78** (1985) 2105–14.
51. Kutschale, H. W., Rapid computation by wave theory of propagation loss in the Arctic Ocean. Report No. CU-8-73. Columbia University, Palisades, New York, 1973.
52. Di Napoli, F. R., Fast field program for multilayered media. NUSC Tech. Report 4103, Naval Underwater Systems Center, 1971.
53. Tappert, F. D., The parabolic approximation method. In *Wave Propagation and Underwater Acoustics*, ed. J. B. Keller & J. S. Papadakis, Springer-Verlag, Berlin, 1977, pp. 224–87.
54. Jensen, F. B. & Krol, H. R., The use of the parabolic equation method in sound propagation modelling. Report No. SM-72, SACLANT ASW Centre, La Spezia, Italy, 1975.
55. Lee, D. & Botseas, G., IFD: an implicit finite-difference computer model for solving the parabolic equation. NUSC Tech. Report No. 6659, New London, CT, 1982.

56. Botseas, G. & Lee, D., IFD: wide angle capability. NUSC Tech. Report No. 6905, New London, CT, 1983.
57. Spofford, C. W., The FACT model, Vol. 1. AESD, Office of Naval Research, Report No. 109, 1974.
58. Yarger, D. F., The user's guide for the RAYMODE propagation loss program. NUSC Tech. Memo. No. 222-10-76, 1976.
59. Keller, J. B. & Papadakis, J. S., *Wave Propagation and Underwater Acoustics*. Springer-Verlag, Berlin, 1977.
60. Brekhovskikh, L. M. & Lysanov, Yu., *Fundamentals of Ocean Acoustics*. Springer-Verlag, Berlin, 1982.
61. Brekhovskikh, L. M., *Waves in Layered Media*. Academic Press, New York, 1980.
62. Weston, D. E., Acoustic flux methods for oceanic guided waves. *J. Acoust. Soc. Am.*, **68** (1980) 287–96.
63. Weston, D. E., Acoustic flux formulas for range-dependent ocean ducts. *J. Acoust. Soc. Am.*, **68** (1980) 269–81.
64. Harrison, C. H. & Ainslie, M. A., The suitability of the WKB method to fast numerical acoustic pressure calculations. In *Acoustics and Ocean Bottom*, ed. A. Lara, C. Ranz & R. Carbo, Federation of the Acoustic Societies of Europe, Imprenta Moderna, 1987.
65. Biot, M. A. & Tolstoy, I., Formulation of wave propagation in infinite media by normal coordinates with an application to diffraction. *J. Acoust. Soc. Am.*, **29** (1957) 381–91.
66. Porter, M. B. & Bucker, H. P., Gaussian beam tracing for computing ocean acoustic fields. *J. Acoust. Soc. Am.*, **82** (1987) 1349–59.
67. Miller, J. F. & Ingenito, F., Normal mode FORTRAN programs for calculating sound propagation in the ocean. NRL Memo. Report No. 3071, 1975.
68. Porter, M. B. & Reiss, E. L., A numerical method for bottom interacting ocean acoustic normal modes. *J. Acoust. Soc. Am.*, **77** (1985) 1760–7.
69. Ferla, M. C., Jensen, F. B. & Kuperman, W. A., High frequency normal-mode calculations in deep water. *J. Acoust. Soc. Am.*, **72** (1982) 505–9.
70. Ingenito, F. & Wolf, S., Acoustic propagation in shallow water overlying a consolidated bottom. *J. Acoust. Soc. Am.*, **60** (1976) 611–7.
71. Kuperman, W. A. & Ingenito, F., Attenuation of the coherent component of sound propagating in shallow water with rough boundaries. *J. Acoust. Soc. Am.*, **61** (1977) 1178–87.
72. Labianca, F. M., Normal modes, virtual modes, and alternative representations in the theory of surface-duct sound propagation. *J. Acoust. Soc. Am.*, **53** (1973) 1137–47.
73. Stickler, D. C., Normal-mode program with both discrete and branch line contributions. *J. Acoust. Soc. Am.*, **57** (1974) 856–61.
74. Bartberger, C., Comparison of two normal-mode solutions based on different branch-cuts. *J. Acoust. Soc. Am.*, **61** (1977) 1643.
75. Williams, A. O. Pseudoresonances and virtual modes in underwater sound propagation. *J. Acoust. Soc. Am.*, **64** (1978) 1487–91.
76. Tindle, C. T., Virtual modes and mode amplitudes near cut off. *J. Acoust. Soc. Am.*, **65** (1979) 1423–8.
77. Tindle, C. T., Stamp, A. & Guthrie, K. M., Virtual modes and the surface boundary condition in underwater acoustics. *J. Sound Vibr.*, **49** (1976) 231–40.

78. Jensen, F. B. & Kuperman, W. A., Sound propagation in a wedge-shaped ocean with a penetrable bottom. *J. Acoust. Soc. Am.*, **67** (1980) 1564–6.
79. St Mary, D. F. & Lee, D. Accurate computation of the wide-angle wave equation. In *Computational Acoustics: Wave Propagation*, ed. D. Lee, R. L. Sternberg & M. H. Schultz. International Association for Mathematics and Computers in Simulation. North-Holland, New York, 1988.
80. Knightly, G. H. & St Mary, D. F., Derivation of higher-order parabolic equations which include density variations. *J. Acoust. Soc. Am.*, **82** Suppl. 1 (1987) UU2.
81. Lee, D., Sternberg, R. L. & Schultz, M. H. (eds), *Computational Acoustics: Wave Propagation*. International Association for Mathematics and Computers in Simulation. North-Holland, New York, 1988.
82. Brent, R. I., Siegmann, W. L. & Jacobson, M. J., Effects of uniform horizontal currents in the parabolic approximation method. *J. Acoust. Soc. Am.*, **82** (1987) 545–58.
83. Robertson, J. S., Siegmann, W. L. & Jacobson, M. J., Acoustical effects of ocean current shear structures in the parabolic approximation. *J. Acoust. Soc. Am.*, **82** (1987) 559–73.
84. Baer, R. N., Perkins, J. S., Wright, E. B. & Adams, B. B., An acoustic model for bathymetric scattering with low-frequency applications. In *Ocean Seismo-Acoustics*, ed. T. Akal & J. M. Berkson. Plenum Press, New York, 1986, pp. 345–53.
85. Baer, R. N., Propagation through a three-dimensional eddy including effects on an array. *J. Acoust. Soc. Am.*, **69** (1981) 70–5.
86. Perkins, J. S. & Baer, R. N., An approximation to the three-dimensional parabolic-equation method for acoustic propagation. *J. Acoust. Soc. Am.*, **72** (1982) 515–22.
87. Jensen, F. B. & Kuperman, W. A., Environmental acoustic modelling at SACLANTCEN. Report SR-34, SACLANT ASW Research Centre, La Spezia, Italy, 1979.
88. Jensen, F. B. & Kuperman, W. A., Consistency tests of acoustic propagation models. Report SM-157, SACLANT ASW Research Centre, La Spezia, Italy, 1982.
89. McDaniel, S. T. & Lee, D., A finite-difference treatment of interface conditions for the parabolic wave equation: the horizontal interface. *J. Acoust. Soc. Am.*, **71** (1982) 855–8.
90. Thompson, D. J. & Chapman, N. R., A wide-angle split-step algorithm for the parabolic equation. *J. Acoust. Soc. Am.*, **74** (1983) 1848–54.
91. Pierce, A. D., Augmented adiabatic mode theory for upslope propagation from a point source in variable-depth shallow water overlying a fluid bottom. *J. Acoust. Soc. Am.*, **74** (1983) 1837–47.
92. Tolstoy, A., Berman, D. H. & Franchi, E. R., Ray theory versus the parabolic equation in a long-range ducted environment. *J. Acoust. Soc. Am.*, **78** (1985) 176–89.
93. Brock, H. K., Buchal, R. N. & Spofford, C. W., Modifying the sound-speed profile to improve the accuracy of the parabolic-equation technique. *J. Acoust. Soc. Am.*, **62** (1977) 543–52.
94. Spofford, C. W., A synopsis of the AESD Workshop on Acoustic Propagation Modeling by Non-Ray-Tracing Techniques. Report TN-73-05, Office of Naval Research, Washington DC, 1973.

95. Davis, J. A., White, D. & Cavanagh, R. C., NORDA Parabolic Equation Workshop. Report TN-143, Naval Ocean Research and Development Activity, NSTL Station, MS, 1982.
96. Quality assessment of numerical codes. Special session in: *J. Acoust. Soc. Am.*, **80**, Suppl. 1 (1986) I, R.
97. Numerical solutions of two benchmark problems. Special session in: *J. Acoust. Soc. Am.*, **81**, Suppl 1 (1987) Q.
98. Tindle, C. T. & Weston, D. E., Connection of acoustic beam displacement, cycle distances and attenuations for rays and normal modes. *J. Acoust. Soc. Am.*, **67** (1980) 1614–22.
99. Fitzgerald, R. M., Helmholtz equation as an initial value problem with application to acoustic propagation. *J. Acoust. Soc. Am.*, **57** (1975) 839–42.
100. McDaniel, S. T., Propagation of normal modes in the parabolic approximation. *J. Acoust. Soc. Am.*, **57** (1975) 307–11.
101. McDaniel, S. T., Parabolic approximations for underwater sound propagation. *J. Acoust. Soc. Am.*, **58** (1975) 1178–85.
102. Palmer, D. R., Eikonal approximation and the parabolic equation. *J. Acoust. Soc. Am.*, **60** (1976) 343–54.
103. Claerbout, J. F., *Fundamentals of Geophysical Data Processing*. McGraw-Hill, New York (1976), pp. 206–7.
104. Thompson, D. J. & Wood, D. H., A post processing method for removing phase errors in the parabolic equation. *J. Acoust. Soc. Am.*, **82** (1987) 224–32.
105. Pierce, A. D., The natural reference wavenumber for parabolic approximations in ocean acoustics. *Comput. Maths. Applics*, **11** (1985) 831–41.
106. Harrison, C. H., A formula for reference sound speed (unpublished).
107. Weston, D. E., Intensity–range relations in oceanographic acoustics. *J. Sound Vibr.*, **18** (1971) 271–87.